

Nanoscale

Accepted Manuscript



This is an *Accepted Manuscript*, which has been through the Royal Society of Chemistry peer review process and has been accepted for publication.

Accepted Manuscripts are published online shortly after acceptance, before technical editing, formatting and proof reading. Using this free service, authors can make their results available to the community, in citable form, before we publish the edited article. We will replace this *Accepted Manuscript* with the edited and formatted *Advance Article* as soon as it is available.

You can find more information about *Accepted Manuscripts* in the [Information for Authors](#).

Please note that technical editing may introduce minor changes to the text and/or graphics, which may alter content. The journal's standard [Terms & Conditions](#) and the [Ethical guidelines](#) still apply. In no event shall the Royal Society of Chemistry be held responsible for any errors or omissions in this *Accepted Manuscript* or any consequences arising from the use of any information it contains.

Study of Exciton Transfer in Dense Quantum Dot Nanocomposites

Burak Guzelturk^{1,2}, Pedro Ludwig Hernandez-Martinez^{1,2}, Vijay Kumar Sharma¹, Yasemin Coskun¹, Vusala Ibrahimova¹, Donus Tuncel¹, Alexander O. Govorov³, Xiao Wei Sun², Qihua Xiong² and Hilmi Volkan Demir^{1,2*}

¹Department of Electrical and Electronics Engineering, Department of Physics, Department of Chemistry, and UNAM–National Nanotechnology Research Center, Institute of Materials Science and Nanotechnology, Bilkent University, Ankara, Turkey TR-06800

² *Luminous!* Center of Excellence for Semiconductor Lighting and Displays, School of Electrical and Electronic Engineering, School of Physical and Mathematical Sciences, Nanyang Technological University, Nanyang Avenue, Singapore 639798, Singapore

³ Department of Physics and Astronomy, Ohio University, Athens, Ohio, 45701, United States

Keywords: Conjugated polymers, colloidal quantum dots, Förster resonance energy transfer, FRET, exciton transfer, exciton diffusion, hybrid light-emitting diodes.

ABSTRACT: Nanocomposites of colloidal quantum dots (QDs) integrated into conjugated polymers (CPs) are key to hybrid optoelectronics, where engineering the excitonic interactions at the nanoscale is crucial. For such excitonic operation, it was believed that exciton diffusion is essential to realize nonradiative energy transfer from the CPs into the QDs. In this study, contrary to the previous literature, efficient exciton transfer is demonstrated in the nanocomposites of dense QDs, where exciton transfer can be as efficient as 80% without requiring the assistance of exciton diffusion. This is enabled by uniform dispersion of QDs at high density (up to ~70 w%) in the nanocomposite while avoiding phase segregation. Theoretical modeling supports the experimental observation of weakly temperature dependent nonradiative energy transfer dynamics. This new finding provides the ability to design hybrid light-emitting diodes that show an order of magnitude enhanced external quantum efficiencies.

Introduction

Colloidal quantum dots (QDs) are prominent materials for optoelectronics with excellent prospects for light generation,¹ light harvesting,² light detection,³ and lasing.⁴ Alternatively, conjugated polymers (CPs) are important class of organic semiconductors that exhibit complementary properties.^{5–7} Nanocomposites integrating both the CPs and the QDs potentially offer a mutual synergy.^{8–11} To this end, engineering excitonic interactions, which crucially depends on the interactions at the nanoscale, is vital for developing hybrid materials for high performance hybrid optoelectronic devices.^{11,12} Fluorescence resonance energy transfer (FRET) from CPs to the QDs was shown to be possible in CP-QD composite systems, which were either mechanically blended or electrostatically integrated.^{13–19} For such energy transfer to occur, exciton diffusion in CP was shown to be essentially required.²⁰ However, exciton diffusion assisted FRET was demonstrated with only low density QD (3 w%) incorporated CP-QD blends in order to prevent phase segregation, which occurs at increased densities of QDs in the CP-QD blends.^{20,21} To date, interplay between exciton transfer and diffusion has not been understood, nor studied for high density QD loaded nanocomposites, which would be inevitable from the technological point of view for the realization of hybrid organic-inorganic optoelectronic devices.

In this work, we systematically study FRET at low and high density QD incorporating nanocomposites and blends achieved via utilization of two different CPs, i.e., functionalized and nonfunctionalized polyfluorene, respectively. These CPs have a similar conjugated backbone but have different side chain groups,

which possess different compatibility with the QDs. Functionalized CP significantly suppresses phase separation in the nanocomposite films when incorporated with high density QDs (up to 70 w%). On the other hand, nonfunctionalized CP exhibits severe phase segregation in the blended films incorporating high density QDs. In these nanocomposites and blends, we investigate FRET at low and high QD density loadings as a function of temperature. In the case of low density QD incorporation, exciton diffusion assisted FRET is the dominant exciton transfer mechanism for both CPs. In the case of high density QD loadings; temperature dependent FRET kinetics are observed to substantially differ between the nanocomposite (functionalized CP-QDs) and the blend (nonfunctionalized CP-QDs). The nanocomposite with high density QDs dominantly exhibits direct exciton transfer, which does not require exciton diffusion assistance. Whereas, the blend with high density QDs exhibits high temperature sensitivity for the FRET kinetics since exciton diffusion assistance is still required due to the aggregate formation of the QDs in the blended films. These exciton diffusion assisted exciton transfer and direct exciton transfer channels are schematically summarized in Figure 1a for the nanocomposite and blend cases at low and high density QDs. Through theoretical energy transfer models, we infer the cooperative and competitive nature between the exciton transfer and the exciton diffusion. In high density QD incorporating nanocomposites exciton diffusion is suppressed by 5-folds as compared to the low density QDs. Finally, we demonstrate hybrid light-emitting diodes that employ the nanocomposites and the blends as the light-emitting layer of the devices. Nanocomposite-LEDs outperform the other devices with a dominant QD emission in their electroluminescence spectra thanks to the efficient energy

transfer pumping, whereas blend-LEDs always exhibit emission from the nonfunctionalized CP due to incomplete energy transfer to the QDs.

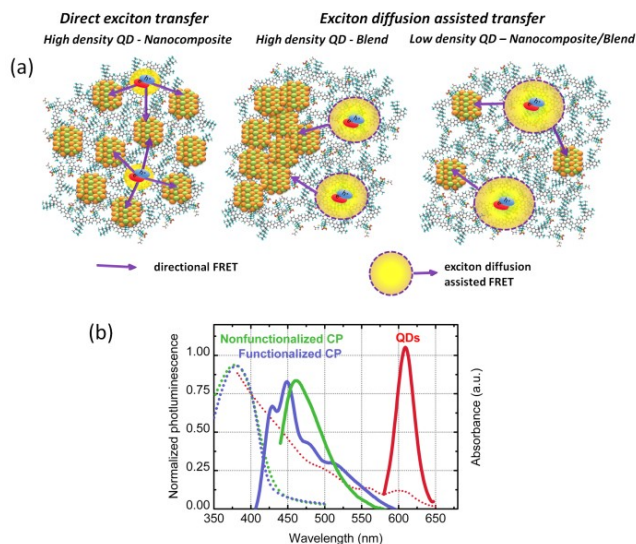


Figure 1. (a) Representative schematic for the exciton transfer at the high density QD incorporating (left) nanocomposite, (middle) blend and the low density QD incorporating (right) nanocomposite and blend. (b) Normalized photoluminescence (solid) and absorbance (dotted) spectra of the functionalized CP, nonfunctionalized CP and the QDs.

Experimental Section

Synthesis of the functionalized polymer

Poly[(9,9-bis(propenyl)fluorenyl-2,7-diyl)-co-(9,9-dihexylfluorenyl-2,7-diyl)] (P1) was synthesized by the Suzuki coupling of 9,9-dihexylfluorene-2,7-bis(trimethyleneborate) and 9,9-bis(propenyl)-2,7-dibromo-9H-fluorene and through thiol-en reaction allyl groups reacted with mercaptoacetic acid to afford poly[(9,9-bis{carboxymethylsulfonyl-propyl}fluorenyl-2,7-diyl)-co-(9,9-dihexylfluorenyl-2,7-diyl)] (functionalized CP). The conversion of allyl to carboxymethylsulfonyl group was confirmed by the presence of characteristic carbonyl bond stretching at 1650 cm^{-1} in IR spectrum of functionalized CP. The weight average molecular weights (Mw) were determined as 9.02 103 g mol^{-1} for P1 by gel permeation chromatography (GPC) using polystyrene as standard. Synthesis of poly[(9,9-bis(propenyl)fluorenyl-2,7-diyl)-co-(9,9-dihexylfluorenyl-2,7-diyl)] (P1)

2,7-dibromo-9,9-bis-(propenyl)-9H-fluorene (1.00 g, 2.474 mmol), 9,9-dihexylfluorene-2,7-bis(trimethyleneborate) (1.243 g, 2.474 mmol) and K_2CO_3 (3.419 g, 24.74 mmol) were dried under vacuum while THF, H_2O and toluene were degassed under Argon about 15 min. Then the mixture was suspended into degassed THF (10 mL), water (10 mL) and toluene (10 mL) and catalyst tetrakis (triphenylphosphine) palladium (0) ($\text{Pd}(\text{PPh}_3)_4$) (0.0286 g, 0.025 mmol) was added quickly. After 3 h phase transfer catalyst tetra-n-butylammonium bromide (TBAB) (0.0079 g, 0.025 mmol) was added and the resulting mixture was stirred under Argon gas for 48 h at 80-90°C. At the end of the reaction, the solvent was evaporated to obtain a solid residue which was suspended in chloroform-water mixture. The organic layer was separated and evaporated to the reduced volume and precipitated into cold methanol (100 mL). The precipitates were collected by suction filtration; washed with water several times and redissolved in a minimum amount of THF. The solution was reprecipitated into excess cold methanol. Light yellow colored precipitates were collected by filtration and dried under vacuum for 6 h.

Yield: 93%

$^1\text{H-NMR}$ (400MHz, CDCl_3 , 25°C), δ 7.85 (m, 8H, Ar H), 5.54 (q, 2H, CH), 5.02 (t, 4H, CH₂), 2.89 (m, 4H, CH₂), 1.54 (q, 4H, CH₂), 1.15 (m, 4H, CH₂), 0.81 (m, 6H, CH₃)

GPC: Mn= 7.01 103 Mw= 9.02 103 (Polystyrene as standard)

Synthesis of poly[(9,9-bis{carboxymethylsulfonyl-propyl}fluorenyl-2,7-diyl)-co-(9,9-dihexylfluorenyl-2,7-diyl)] (functionalized CP)

Poly[(9,9-bis{propenyl}fluorenyl-2,7-diyl)-co-(9,9-dihexylfluorenyl-2,7-diyl)] (P1) was dissolved in CHCl_3 and excess mercaptoacetic acid was added. The mixture was stirred under reduced pressure and dissolved in THF and the resulting solution was precipitated into water to yield light yellow color functionalized CP, which was dried under vacuum for 6 h.

Synthesis of the core-shell QDs

For the growth of CdSe cores, the synthesis started with mixing 64 mg of cadmium oxide (CdO), 183.5 mg of zinc acetate (ZnAc) and 2.5 mL of oleic acid (OA). Under air free environment by using vacuum conditions, the mixture was heated up to 150°C, waiting for 30 minutes at this temperature. Then, the system was taken from vacuum to argon flow and 12.5 mL of degassed 1-octadecene (ODE) was added quickly into the prepared mixture. After addition of ODE, the temperature of the system was increased to 300°C. At the reported elevated temperature, 0.1 mL of injection solution of selenium (Se), which was prepared as 1M in trioctylphosphine (TOP), was injected quickly into the clear reaction mixture, and the core growth continued for 2.5 min. Subsequently, 0.15 mL of dodecanethiol (DDT) was added slowly at the rate of 1 mL/min. After waiting for 20 min for the formation of CdZnS layer overcoating the cores, 0.5 mL of injection solution of sulphur (S), prepared as 2M in TOP, was added into the reaction mixture quickly. For the formation of final ZnS shell, 10 min growth time was used. At the end of the synthesis, the solution was cooled down to room temperature to stop the growth. These QDs in solution have photoluminescence quantum efficiencies up to 50%.

Hybrid film preparation

20 mg/mL of functionalized CP in THF and 10 mg/mL of core/shell QDs in toluene were mixed in desired ratio. The mixture is left in vortex overnight. Subsequently, the mixture was spin-coated using 2000 rpm for 1.5 min. The resulting thin film thickness was measured to be 60 nm using a profilometer.

SEM and TEM characterization

Scanning electron microscopy (Quanta 200 FEG, FEI) of the nanocomposite and blend films spin-coated on (100) p-doped silicon substrates was carried out. Energy dispersive X-ray spectrometer integrated with SEM system (EDAX, Materials Analysis Division) was used to understand the phase segregated parts of the blended films. Transmission electron microscopy (Technai G2 F30, FEI) was used with ultra thin carbon grids in scanning mode via high sensitivity HAADF STEM detector.

Time resolved fluorescence spectroscopy

Time resolved fluorescence spectrometer (Fluotime 200) with time correlated single photon counting system (TCSPC) (Pico Harp 300) integrated with a closed cycle He cryostat was used for measuring the fluorescence decays. A picosecond pulsed laser working at 375 nm operated at 5 MHz repetition rate with an average optical power level of 0.5 mW/cm^2 was utilized. The instrument response function of the system has a full width at half maxima around 200 ps.

Device fabrication

The device fabrication started with the substrate preparation. We used square glass/ITO substrates with 15 Ω /sq sheet resistance (Kintec) of 1.5 cm x 1.5 cm in size. First, we etched the side of the ITO using acidic etchant mixture HCl:HNO₃:H₂O (4.6 : 0.4 : 5). Then, we cleaned substrates using solvent cleaning (deionized water-detergent (Hellmanex III, HellmaAnalytics) mixture, deionized water, acetone, and isopropanol for 15 min each). After the solvent cleaning, substrates were UV-Ozone treated right before spin-coating PEDOT:PSS (using 500, 4000 and 5000 rpms for 5, 120 and 120 s, respectively). Then, the films were annealed in a glove box at 140°C for 2 hours. After, the mixture of hybrid solution was prepared and mixed with a vortex for a few hours. The hybrid solution was spin-coated at 2000 rpm for 2 min. The active layer was annealed at 70°C. In a thermal evaporator, 100 nm thick Al film was deposited. Later, devices were encapsulated with a cover glass using epoxy.

Results and Discussion

In the CP-QD systems phase segregation causes QDs to form aggregates in the CP host; therefore, suppresses FRET from the CP to the QDs since interaction between donor and acceptor is considerably limited. For this reason, phase segregation should be minimized for efficient energy transfer pumping to the QDs from the CPs. There were several reports on developing chemically integrated CP-QD nanocomposites.^{10,22,23} Among these, grafting the CPs to the QD surface via active moieties of the side-chains of the CPs is a versatile method without impairing the original photophysical properties of the QDs.²³ Previously, such grafted CP-QD composites were used for hybrid solar cells²⁴ or light-emitting diodes.^{25–27} However, these nanocomposites were not specifically studied for their spectroscopic properties, nor exciton transfer was understood. In this work, a functionalized CP (poly[(9,9-bis[carboxymethylsulfonyl-propyl]fluorenyl-2,7-diyl)-co(9,9dihexylfluorenyl-2,7-diyl)]) is synthesized (see Figure S1), which has carboxymethylsulfonyl functionalized side groups to interact specifically with the QD surfaces. Nonfunctionalized CP (poly[(9,9-dioctylfluorenyl-2,7-diyl)-co-(N,N'-diphenyl)-N,N'-di(p-butyl-oxy-phenyl)-1,4-diaminobenzene]) – American dye source 232 GE) has a similar backbone compared to the functionalized CP, yet it does not have any specific active side-chain moieties. As the QDs, we synthesize red-emitting core/shell CdSe/ZnS QDs having average diameter of 6.3 nm (see Figure S2 for the TEM images).²⁸ Figure 1b depicts the fluorescence emission and absorbance of the functionalized and nonfunctionalized CPs and the QDs.

Suppression of the phase segregation

Thin films of the functionalized CP-QD nanocomposites and the nonfunctionalized CP-QD blends were fabricated via spin coating over cleaned quartz substrates. Two different QD concentrations were used; low density (QD : CP = 3 w% : 97 w%) and high density (QD : CP = 45 w% : 55 w%). For the case of high density QDs in functionalized CP scanning electron microscopy (SEM) image in Figure 2a does not exhibit any indication phase segregation at a resolution level of a few hundred nanometers, whereas Figure 2c depicts SEM image of the blend with high density QDs, where severe phase segregation is clearly visible. Figure 2b shows the high-angle annular dark-field scanning transmission electron microscopy (HAADF STEM) image of the high density QD loaded nanocomposite that reveals suppressed phase segregation owing to the presence of the active carboxyl acid moieties at the side chains of the functionalized CP, which act as multi-ligands for the QDs (see Supporting Information for the XPS analysis that reveal the strong interaction with the side chains of the functionalized CP with the QD surface). In addition,

we always observe amorphous cloud around the QDs in HAADF-STEM images having darker color than the carbon grid background, which is possibly attributed to surrounding functionalized CPs around the QDs. However, this darker colored cloud is never observed for the same QDs when mixed with nonfunctionalized CP (see Figure 2d).

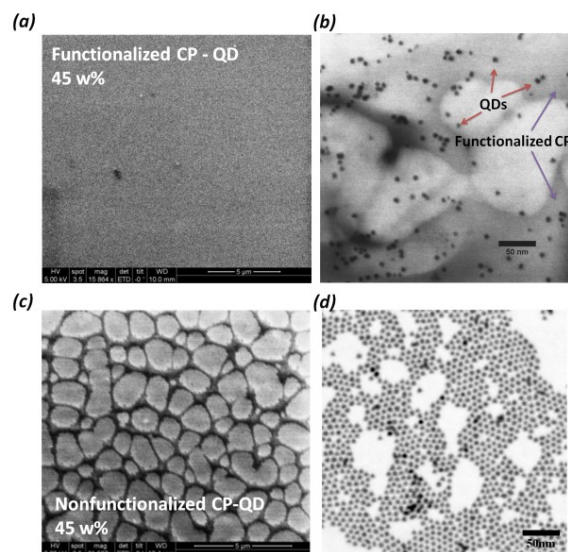


Figure 2. Scanning electron microscopy (SEM) of (a) the functionalized CP-QD nanocomposite and (c) the nonfunctionalized CP-QD blend with the same QD density of 45 w%. High-angle annular dark-field scanning transmission electron microscopy (HAADF STEM) images of (b) the functionalized CP-QD nanocomposite and (d) the nonfunctionalized CP-QD blend with the same QD density of 45 w%.

Temperature dependent energy transfer dynamics

Time correlated single photon counting (TCSPC) technique is employed to measure the fluorescence decay kinetics of the donor CPs. In the absence of QDs, the fluorescence decays of the CPs are fitted well using single exponential decay function with a near-unity reduced χ^2 after deconvoluting with the instrument response function. To compute the FRET efficiencies (η) in the case of the blends, we employ the fitted amplitude averaged fluorescence lifetimes of the CP in the absence (τ_{CP}) and presence

(τ_{CP-QD}) of the QDs ($\eta = 1 - \frac{\tau_{CP-QD}}{\tau_{CP}}$). For the nanocomposites,

we apply Loring-Anderson-Fayer (LAF) approach to analyze the fluorescence decays.^{20,29} LAF method extends decay kinetics described by Förster theory for multi-acceptors in the three-dimension.³⁰ Supporting Information describes the LAF approach in more detail. The FRET efficiencies are calculated using Equation (S8). Figure 3a and Figure 3b plots the FRET efficiencies as a function of temperature for the nanocomposite and the blend at 3 w% and 45 w% density QD loadings. Low density QD incorporation into both CPs lead to highly temperature sensitive FRET kinetics. This observation is in accordance with the essentially exciton diffusion assisted FRET process.²⁰ Exciton diffusion in a CP is suppressed at low temperatures due to absence of thermal activation energy³¹; therefore, FRET from the CP to the QDs is consequently suppressed (<150 K). Even negative FRET efficiencies are calculated in the blend. We attribute the negative FRET efficiencies at the cryogenic temperatures to the possible morphological phase change of the nonfunctionalized CP at low temperatures, which alters the excited state relaxation dynamics of the CP. Also, this phase change may take place differently in the presence

of the QDs leading to the calculation of negative FRET efficiencies as also observed previously.^{19,20,32}

A fundamental difference in temperature-dependent FRET kinetics is observed in the case high density QD loadings. In the nanocomposite with high density QDs, FRET efficiencies are observed to exhibit much weaker temperature sensitivity (see Figure 3a). More than 80% of the FRET efficiency at room temperature is sustained even at the lowest temperature case of 37 K. This affirms that exciton diffusion is not critically assisting FRET in the nanocomposite with high density QDs. Thus, direct exciton transfer from the functionalized CP to the QDs is viable. Nonetheless, in the blend at high density QDs, temperature sensitivity of FRET is still high similar to its low density QD loaded counterpart (see Figure 3b). At the lowest temperature, less than 30% of the room temperature FRET efficiency could be sustained in the blend with high density QDs. This is due to the fact that aggregation of the QDs in the blend inhibits the direct exciton transfer and exciton diffusion assistance is still required.

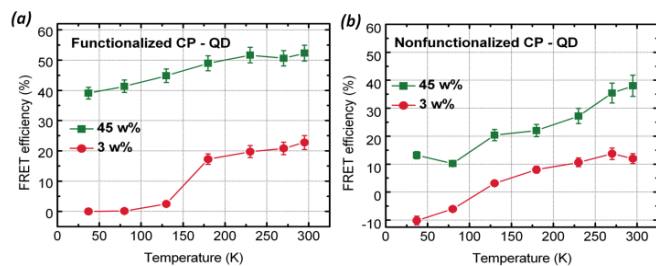


Figure 3. Temperature dependent FRET efficiencies are represented for the 3 and 45 w% density QD incorporating (a) nanocomposite and (b) blend.

Energy transfer models: Exciton transfer vs. Exciton diffusion

We model the exciton transfer and the exciton diffusion dynamics in the nanocomposites using Gösele approach.³³ Contribution from the exciton diffusion is explicitly included in the Gösele model to account for the exciton diffusion assistance to FRET (see Supporting Information for more details about the Gösele Model). Here, we do not consider the blend cases since it is difficult to consider the effects of random aggregates that are observed in the blends at high density QD loadings. Equation (S9) relates the donor fluorescence lifetime that is modified due to the presence of acceptor. In this equation, diffusion coefficient (D , in units of nm^2/ns) is the only unknown parameter. Density of the acceptors (n_A , in units of $\#\text{QDs}/\text{nm}^3$) is estimated in the nanocomposites via measuring the absorbance of the QDs in the hybrid films and comparing them with the known concentration solutions of the QDs. n_A is $\sim 4.0 \times 10^{-5}$ QDs/ nm^3 and $\sim 3.6 \times 10^{-4}$ QDs/ nm^3 for the cases of 3 w% and 45 w% density QDs, respectively. Then, we model the donor fluorescence lifetime of the functionalized CP using Equation (S9) parameterized with respect to D and n_A . In the Supporting Information we present the analysis to cross-check Gösele approach by calculating the time expected value of τ_{DA} using Equation (S12) as shown in Figure S4, where time expected value of the modeled donor fluorescence lifetimes match very well with the experimental donor fluorescence lifetimes. Figure 4a and Figure 4b plot the iso-fluorescence lifetime (iso- τ_{DA}) of the donor, i.e., functionalized CP, in the presence of acceptors at two exemplary temperature points of 295 K and 180 K, respectively. Iso-fluorescence lifetimes are shown for the rest of the temperature points in Figure S5. In Figure 4a and Figure 4b, modeled iso- τ_{DA} curves are plotted with varying color shades, where τ_{DA} becomes longer as the shades vary from light brown to darker brown color. It is observed that increasing either

n_A and D favors a decrease of τ_{DA} since increase in these parameters (i.e., D and n_A) favors an increased FRET rate from the CP to the QD. In each Figure 4a and 4b, two iso- τ_{DA} curves are made bold, which represent the experimental τ_{DA} (i.e., 0.097 ns and 0.057 ns in Figure 4a for 45 w% and 3 w% density QD loaded nanocomposite, respectively). We mark the D values by horizontal dashed lines (red color for 3 w% and green color for 45 w%), which match the modeled- τ_{DA} to the experimental τ_{DA} for the given n_A at the low or high density QD incorporating nanocomposites.

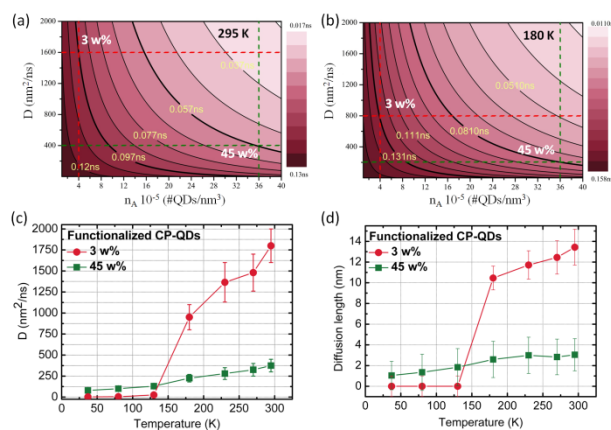


Figure 4. Iso- τ_{DA} curves, modeled by Gösele approach, are plotted as a function of D and n_A at (a) 295 and (b) 180 K. Diffusion coefficient, D , which matches the modeled- τ_{DA} to the experimental- τ_{DA} , is highlighted by red and green dashed line for 3 w% and 45 w% QD loading, respectively. (c) D as a function of temperature for the 3 and 45 w% density QD loaded nanocomposites. (d) Diffusion length (L_D) as a function of temperature for the cases of 3 and 45 w% QD loaded nanocomposites.

Figure 4c shows the diffusion coefficients (D) that are extracted by matching the modeled iso- τ_{DA} to the experimental τ_{DA} using Gösele model. Here, we observe a remarkable difference in the exciton diffusion characteristics of the functionalized CP depending on the density of the QD loading. At room temperature, D is found to be $1800 \text{ nm}^2/\text{ns}$ for the 3 w% QD loaded nanocomposite, whereas D is only $350 \text{ nm}^2/\text{ns}$ for 45 w% QD loaded nanocomposite. Higher diffusion coefficient in the low QD density loaded nanocomposite is in agreement with the D of a similar type of polyfluorene derivative polymer, which was found to have $1440 \pm 250 \text{ nm}^2/\text{ns}$ at room temperature.³⁴ This indicates that intrinsic exciton diffusion property of the functionalized CP is preserved in the case of low density QDs in the nanocomposite. However, in the high density QD incorporating nanocomposite, D is observed to be much smaller as compared to the D in the case of low density case. This indicates that exciton diffusion is slowed down due to the incorporation of larger amount of QD incorporation into the nanocomposite. As shown in Figure 4c, D is found to be decreased by 5-folds in the 45 w% nanocomposite as compared to the 3 w% nanocomposite. One possibility to explain this result is to refer to the two fundamental mechanisms of exciton diffusion in the CPs, so called inter- and intra-chain exciton diffusion. The inter-chain diffusion has been shown to be much faster process than the intra-chain diffusion, and the inter-chain diffusion was claimed to be dominant in highly stacked solid-state films of the CPs due to close packing of the polymer chains.^{35,36} On the other hand, the intra-chain diffusion becomes dominant when the CP chains are more isolated as in the case of dilute solutions. Thus, the decrease of diffusion coefficient at high QD densities can be possibly attributed to the morphological changes in the

polymer matrix. The CP chains are more isolated from each other in the case of high density nanocomposite as compared to low density case. Hence, slower intra-chain diffusion may dominate as opposed to faster inter-chain diffusion.

The temperature dependent change of the D in low and high density QD cases is also different. As the temperature is reduced from room temperature down to 150 K, D is reduced substantially in the case of low QD density nanocomposite. There is a turn-off temperature below 150 K as observed before.²⁰ However, in the case of high density nanocomposite there is a monotonic decrease of the D as the temperature is decreased. Exciton diffusion in the CPs is a temperature activated process that takes place via hopping of the excitons over different units of the polymer chains, where the extra energy (i.e., kT) is required to jump over the low energy traps in the disordered density of states (DOS) of the CP.³⁵ Therefore, decrease of the D as the temperature is reduced is expected. Yet, behavior below 150 K may be attributed to changing conformation and inter-chain packing of the polymer at the cryogenic temperatures, which is only observed for the low QD incorporated nanocomposites. In the case of high QD loading, exciton diffusion is highly slowed down.

In Figure 4d we plot the exciton diffusion length ($L_D = \sqrt{D\tau_D}$) in the nanocomposites of low and high density QDs using the estimated diffusion coefficient D (Figure 4c) and the experimentally known fluorescence lifetime of the CP. L_D also exhibits significant difference between the low and the high density nanocomposites. For the low density, L_D is found to be up to 13 nm at room temperature, whereas for the high density L_D is only up to 3 nm. Thus, excitons can on the average diffuse up to 4-fold longer distances in the case of the low density nanocomposite as compared to the high density one. The exciton diffusion length that is slightly larger than 10 nm is in agreement with the previous literature for similar type of polymers.³⁷ This indicates that small amount of QD incorporation into the nanocomposite does not severely disturb the exciton diffusion properties of the CP. However, in the case of high density QDs, exciton diffusion length is very limited (1-3 nm); thus, exciton diffusion is suppressed in the high density QD integrating nanocomposite. This suppressed exciton diffusion is in accordance with only-downhill exciton diffusion in the CPs, where downhill relaxation of the exciton in the disordered density of states of the CPs is estimated to be 2.0 - 2.5 nm.³⁷ Therefore, for the high density QD incorporating nanocomposite, excitons are transferred to the QDs after only-downhill diffusion of the energetic excitons in the disordered DoS of the CP. We present steady state fluorescence measurements of the nanocomposites as a function of temperature as an additional proof of the change of the exciton diffusion properties with QD loading in the nanocomposite in Figure S6, which reveals the spectroscopic signature of the exciton diffusion suppression in the CP emission at high density QD loading.

Exciton transfer efficiency vs. QD loading

To reveal the potential of these functionalized CP-QD nanocomposites as an efficient exciton transferring media, we further study FRET efficiencies in the nanocomposites as a function of varying density of QDs at room temperature as shown in Figure 5a. FRET efficiencies can be as high as 80% when the density of QDs is as high as 70 w%. Here, steady state photoluminescence of the 70 w% density QD loaded nanocomposite is also plotted with its control group samples (bare donor and acceptor) in Figure 5b, where quenching of the CP's fluorescence emission and concomitant enhancement of the QD's fluorescence emission is clearly visible. The fluorescence emission of the QDs

is red-shifted in the nanocomposite as attributed to the better spectral overlap of the slightly larger QDs in the inhomogeneously broadened size distribution. Another proof for this efficient exciton transfer is shown by Figure S3, where fluorescence decay of the QDs in the nanocomposite and the bare QDs are plotted. The fluorescence lifetime of the QDs increases when QDs are in the nanocomposite as compared to the fluorescence decay of the bare QDs. This can be explained by the exciton feeding from the CP donor.^{12,38-40} Also, better surface passivation of the QDs within the nanocomposite might have helped. Moreover, charge transfer from the CP to the QDs is not possible in our system due to the thick ZnS shell (>3 monolayers) of the QDs.⁴¹ Therefore, inter-QD FRET⁴² or inter-QD exciton coupling⁴³ is expected to be quite weak in our case. Previously, Lutich et al. have not even observed significant charge transfer from a similar type of CP to core only CdTe QDs.¹⁷

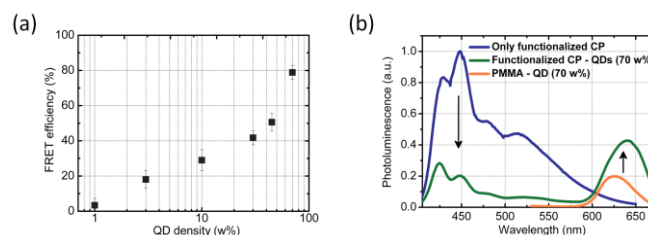


Figure 5. (a) FRET efficiencies are measured as a function of QD density in the hybrid nanocomposite at room temperature. QD densities of 3 w% and 45 w% corresponds to average QD-to-QD distance of 16 and 7 nm in their nanocomposites, respectively. (b) Steady state photoluminescence of only functionalized CP, functionalized CP-QD (70 w%) and PMMA-QD (70 w%).

Exciton transfer pumped hybrid LEDs

Finally, a proof-of-concept demonstration of the CP-QD system as a light-emitting media for light-emitting diodes is presented. Devices are fabricated using a simple device architecture consisting of ITO/PEDOT:PSS/Emissive Layer/Al, where emissive layer consisted of either the bare CPs, the bare QDs, the nanocomposites or the blends. For the nanocomposite-based LEDs, i.e., nanocomposite-LEDs, high density QDs up to 70 w% is employed to facilitate efficient FRET for a strong energy transfer pumping to the QDs from the functionalized CP. In the case of blend-LEDs, strong energy transfer pumping could never be achieved since phase segregation is inevitable. The bare QD-LEDs (without any polymer host) exhibited weak electroluminescence (EL) due to the poor electrical injection in the simple device architecture employed here. On the other hand, nanocomposite-LEDs demonstrated highly stable and enhanced EL spectra with a dominant QD emission as shown in Figure 6a. In these nanocomposite-LEDs, emission of the functionalized CP is substantially suppressed owing to the efficient exciton transfer into the QDs. Although we have previously measured 80% FRET efficiency at 70 w% density QD loaded nanocomposite (see Figure 5a), the observation of almost totally suppressed emission from the CP could be also due to the change of the exciton transfer pathways in the electroluminescent devices. In contrast, blend-LEDs always exhibit mixed emission both from the QDs and the nonfunctionalized CP in their EL spectra (Figure 6a) due to limited and incomplete energy transfer pumping in these phase separated structure. In terms of the external quantum efficiencies (EQE) of the devices, nanocomposite-LEDs enable a significant enhancement, which is more than an order of magnitude, in EQEs as compared to bare QD-LEDs and bare functionalized CP-LEDs as depicted in Figure 6b. Bare QD-LEDs suffer considerably from

the poor charge injection and bare functionalized CP-LEDs suffer from the defects that are highly populated due to the exciton diffusion.⁴⁴ Therefore, in the nanocomposite-LEDs, excitation energy in the CP could be much more effectively utilized through transferring them to the QDs resulting in substantially enhanced EQEs. With careful design of the device architecture, we believe that these excitonic nanocomposites will be promising for high efficiency hybrid LEDs in the future.

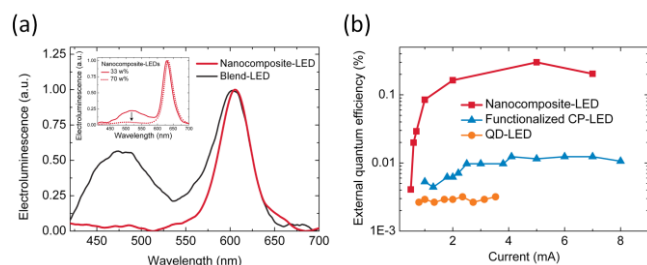


Figure 6. (a) Normalized electroluminescence spectra of the nanocomposite-LED and blend-LED having 70 w% density QDs. The inset shows the normalized electroluminescence spectra of the nanocomposite-LEDs with two different QD densities of 33 w% and 70 w%. (b) External quantum efficiency of the nanocomposite-LED, bare functionalized CP-LED and bare QD-LED.

Conclusion

In conclusion, we study and reveal the excitonic interactions in the conjugated polymer – quantum dot hybrid nanocomposites and blends at low and high density QDs. For such exciton transfer process, it was believed that exciton diffusion is crucially assisting FRET. Here, we reveal the unknown territory of high density QD incorporating nanocomposites. With the help of side-chain functionalized CP, we achieve phase segregation suppressed nanocomposite hybrid films, which show highly efficient exciton transfer (as high as 80%) even at low temperatures. In these high density QD incorporating nanocomposites exciton diffusion assistance to exciton transfer is not required. Instead, direct exciton transfer channel prevails. We employed energy transfer models to explain the interplay between the exciton transfer and the exciton diffusion. At high QD densities, exciton diffusion coefficient is shown to be suppressed by 5-folds. This new understanding and finding is applied to design efficient energy transfer pumped hybrid LEDs that show an order of magnitude enhanced performance.

ACKNOWLEDGMENT

This work is supported in part by EU-FP7 Nanophotonics4Energy NoE, and TUBITAK EEEAG 109E002, 109E004, 110E010, and 110E217, in part by NRF-CRP-6-2010-02 and NRF-RF-2009-09. H.V.D. acknowledges support from ESF-EURYI and TUBA-GEBIP; A.O.G. was supported by U.S. Army Research Office (USA) under grant number W911NF-12-1-0407.

NOTES AND REFERENCES

Corresponding Author

*Address correspondence to: volkan@bilkent.edu.tr, hvdemir@ntu.edu.sg

Electronic Supplementary Information (ESI) available: [Information about the functionalized polymer structure, TEM of the

QDs, XPS analysis of the nanocomposites, derivation of the energy transfer models and temperature dependent steady state PLs].

REFERENCES

1. Y. Shirasaki, G. J. Supran, M. G. Bawendi, and V. Bulović, *Nat. Photonics*, 2013, **7**, 933–933.
2. E. H. Sargent, *Nat. Photonics*, 2012, **6**, 133–135.
3. G. Konstantatos, M. Badioli, L. Gaudreau, J. Osmond, M. Bernechea, F. P. Garcia de Arquer, F. Gatti, and F. H. L. Koppens, *Nat. Nanotechnol.*, 2012, **7**, 363–8.
4. C. Dang, J. Lee, C. Breen, J. S. Steckel, S. Coe-Sullivan, and A. Nurmikko, *Nat. Nanotechnol.*, 2012, **7**, 335–339.
5. J. H. Burroughes, D. D. C. Bradley, A. R. Brown, R. N. Marks, K. Mackay, R. H. Friend, P. L. Burns, and A. B. Holmes, *Nature*, 1990, **347**, 539–541.
6. N. S. Sariciftci, L. Smilowitz, A. J. Heeger, and F. Wudl, *Science*, 1992, **258**, 1474–6.
7. H. Koezuka, A. Tsumura, and T. Ando, *Synth. Met.*, 1987, **18**, 699–704.
8. W. U. Huynh, J. J. Dittmer, and A. P. Alivisatos, *Science*, 2002, **295**, 2425–7.
9. V. L. Colvin, M. C. Schlamp, and A. P. Alivisatos, *Nature*, 1994, **370**, 354–357.
10. P. Reiss, E. Couderc, J. De Girolamo, and A. Pron, *Nanoscale*, 2011, **3**, 446–89.
11. N. Tessler, V. Medvedev, M. Kazes, S. Kan, and U. Banin, *Science*, 2002, **295**, 1506–8.
12. B. Guzelturk, P. L. H. Martinez, Q. Zhang, Q. Xiong, H. Sun, X. W. Sun, A. O. Govorov, and H. V. Demir, *Laser Photon. Rev.*, 2014, **8**, 73–93.
13. , and M. Lomascolo, *Appl. Phys. Lett.*, 2004, **85**, 4169.
14. T.-W. F. Chang, S. Musikhin, L. Bakueva, L. Levina, M. A. Hines, P. W. Cyr, and E. H. Sargent, *Appl. Phys. Lett.*, 2004, **84**, 4295.
15. P. T. K. Chin, R. A. M. Hikmet, and R. A. J. Janssen, *J. Appl. Phys.*, 2008, **104**, 013108.

16. S. Kaufmann, T. Stoferle, N. Moll, R. F. Mahrt, U. Scherf, A. Tsami, D. V. Talapin, and C. B. Murray, *Appl. Phys. Lett.*, 2007, **90**, 071108.
17. A. A. Lutich, G. Jiang, A. S. Sussha, A. L. Rogach, F. D. Stefani, and J. Feldmann, *Nano Lett.*, 2009, **9**, 2636–40.
18. J. H. Warner, A. R. Watt, E. Thomsen, N. Heckenberg, P. Meredith, and H. Rubinsztein-Dunlop, *J. Phys. Chem. B*, 2005, **109**, 9001–9005.
19. A. A. Lutich, A. Poschl, G. Jiang, F. D. Stefani, A. S. Sussha, A. L. Rogach, and J. Feldmann, *Appl. Phys. Lett.*, 2010, **96**, 083109.
20. T. Stoferle, U. Scherf, and R. F. Mahrt, *Nano Lett.*, 2009, **9**, 453–456.
21. N. Greenham, X. Peng, and A. Alivisatos, *Phys. Rev. B*, 1996, **54**, 17628–17637.
22. N. Tomczak, D. Jańczewski, M. Han, and G. J. Vancso, *Prog. Polym. Sci.*, 2009, **34**, 393–430.
23. N. Tomczak, R. Liu, and J. G. Vancso, *Nanoscale*, 2013, **5**, 12018–32.
24. D. J. Milliron, A. P. Alivisatos, C. Pitois, C. Edder, and J. M. J. Fréchet, *Adv. Mater.*, 2003, **15**, 58–61.
25. H. Skaff, K. Sill, and T. Emrick, *J. Am. Chem. Soc.*, 2004, **126**, 11322–5.
26. J. Kwak, W. K. Bae, M. Zorn, H. Woo, H. Yoon, J. Lim, S. W. Kang, S. Weber, H.-J. Butt, R. Zentel, S. Lee, K. Char, and C. Lee, *Adv. Mater.*, 2009, **21**, 5022–5026.
27. M. Zorn, W. K. Bae, J. Kwak, H. Lee, C. Lee, R. Zentel, and K. Char, *ACS Nano*, 2009, **3**, 1063–8.
28. W. K. Bae, K. Char, H. Hur, and S. Lee, *Chem. Mater.*, 2008, **20**, 531–539.
29. R. Loring, H. Andersen, and M. Fayer, *J. Chem. Phys.*, 1982.
30. J. R. Lakowicz, *Principles of Fluorescence Spectroscopy*, 2007.
31. F. B. Dias, K. T. Kamtekar, T. Cazati, G. Williams, M. R. Bryce, and A. P. Monkman, *ChemPhysChem*, 2009, **10**, 2096–2104.
32. X. Zhang, Z. Li, and G. Lu, *Phys. Rev. B*, 2011, **84**, 235208.
33. U. Gösele, M. Hauser, U. Klein, and R. Frey, *Chem. Phys. Lett.*, 1975, **34**, 519–522.
34. U. Scherf and D. Neher, *Polyfluorenes*, 2008.
35. D. Beljonne, G. Pourtois, C. Silva, E. Hennebicq, L. M. Herz, R. H. Friend, G. D. Scholes, S. Setayesh, K. Mullen, and J. L. Bredas, *Proc. Natl. Acad. Sci. U. S. A.*, 2002, **99**, 10982–7.
36. V. Gulbinas, I. Mineviciute, D. Hertel, R. Wellander, A. Yartsev, and V. Sundstrom, *J. Chem. Phys.*, 2007, **127**, 144907.
37. J.-L. Brédas and R. Silbey, *Science*, 2009, **323**, 348–9.
38. E. Mutlugun, P. L. Hernandez-Martinez, C. Eroglu, Y. Coskun, T. Erdem, V. K. Sharma, E. Unal, S. K. Panda, S. G. Hickey, N. Gaponik, A. Eychmüller, and H. V. Demir, *Nano Lett.*, 2012, **12**, 3986–93.
39. - , E. Mutlugun, D. Ugur Karatay, and H. Volkan Demir, *Appl. Phys. Lett.*, 2012, **100**, 241109.
40. P. L. Hernández-Martínez, A. O. Govorov, and H. V. Demir, *J. Phys. Chem. C*, 2013, **117**, 10203–10212.
41. S. Nizamoglu, B. Guzelturk, D.-W. Jeon, I.-H. Lee, and H. V. Demir, *Appl. Phys. Lett.*, 2011, **98**, 163108.
42. C. Kagan, C. Murray, M. Nirmal, and M. Bawendi, *Phys. Rev. Lett.*, 1996, **76**, 1517–1520.
43. M. Artemyev, A. Bibik, L. Gurinovich, S. Gaponenko, and U. Woggon, *Phys. Rev. B*, 1999, **60**, 1504–1506.
44. L. Romaner, A. Pogantsch, P. Scandiucci de Freitas, U. Scherf, M. Gaal, E. Zojer, and E. J. W. List, *Adv. Funct. Mater.*, 2003, **13**, 597–601.

Table of Contents Figure

Direct or exciton diffusion assisted exciton transfer in the varying density colloidal quantum dot incorporated hybrid conjugated polymer nanocomposites.

